Complex Permeability of Fe-deficient Ni-Cu-Zn Ferrites

Z.H. Khan, M. Mahbubur Rahman, S.S. Sikder, M.A. Hakim, D.K Saha

PII: S0925-8388(12)01605-2
DOI: http://dx.doi.org/10.1016/j.jallcom.2012.09.037
Reference: JALCOM 26923

To appear in:

Received Date: 5 August 2012
Revised Date: 8 September 2012
Accepted Date: 10 September 2012

Please cite this article as: Z.H. Khan, M. Mahbubur Rahman, S.S. Sikder, M.A. Hakim, D.K Saha, Complex Permeability of Fe-deficient Ni-Cu-Zn Ferrites, (2012), doi: http://dx.doi.org/10.1016/j.jallcom.2012.09.037

Complex Permeability of Fe-deficient Ni-Cu-Zn Ferrites

Z.H. Khan[1], M. Mahbubur Rahman[2,3], S.S. Sikder[4], M.A. Hakim[5], D.K Saha[5]

[1]Department of Physics, Phultala M.M. College, Phultala, Khulna- 9210, Bangladesh.

[2]School of Engineering & Energy, Murdoch University, Murdoch, WA-6150, Australia.

[3]Department of Physics, Jahangirnagar University, Savar, Dhaka-1342, Bangladesh.

[4]Department of Physics, Khulna University of Engineering & Technology, Khulna- 9203, Bangladesh.

[5]Materials Science Division, Atomic Energy Centre, Ramna, Dhaka- 1000, Bangladesh.

Abstract

Fe-deficient *Ni-Cu-Zn* ferrites with composition $Ni_{0.28}Cu_{0.10}Zn_{0.62}O(Fe_2O_3)_{1-x}$, where x = 0.00, 0.02, 0.04, 0.06 and 0.08 were prepared by the double sintering ceramic technique. Real part of the initial permeability μ', Curie temperature T_c, imaginary part of the initial permeability μ'', relative quality factor (Q-factor) of the samples were elaborately discussed as a function of frequency and temperature with increase of Fe-deficiency during the heating and cooling cycles. The temperature dependence of the imaginary part of the complex permeability curves are very interesting to note that there is a peak value of μ'' at particular temperature which corresponds to the T_c because at this temperature the samples might be in complete spin disorder. This reflects that at T_c, a ferrimagnetically ordered state over comes K_BT and becomes comparable with μ_0H where the loss becomes maximum. Results of heating and cooling cycles were found to be very close to each other. The small difference during heating and cooling process might arise due to the thermal hysteresis which is accumulated in this work. In our study, it was noticed that the resonant frequency and T_c increases first with the increase in iron deficiency and decreases after it takes a maximum at x = 0.06.

Key Words: Iron deficient, initial permeability, relative quality factor, complex permeability, ferromagnetically ordered.

Corresponding author: mahbub235@yahoo.com (M. Mahbubur Rahman)

Introduction

Polycrystalline soft ferrites prepared from metal oxides are magnetic semiconductors and have made important contributions both technological and conceptual development of electronics and electronic industries. Up until today, soft ferrites remain the best magnetic materials which are irreplaceable by any other magnetic materials with respect to their very high frequency applications because they are inexpensive, more stable, easily manufactured [1]. They have wide variety of technological applications in transformer cores, inductors, high quality filters, radio frequency circuits, rod antennas, read/write heads for high-speed digital tape and operating devices as well [2-4].

Properties of soft ferrites are highly sensitive to preparation method, sintering conditions, amount of constituent metal oxides, various additives including dopants and impurities [5-8]. Among soft ferrites, *Ni-Zn*, *Mg-Zn* and *Mn-Zn* ferrites with various additives have enormous technological applications and accordingly extensive research have been carried out by many groups around the globe [9-13]. It is known that ferrites crystallize with two magnetic sub-lattices i.e., tetrahedral (A) sites and octahedral (B) sites based on Neel's model. Various properties of ferrites are strongly dependent on cationic distributions in A and B sites and their valency state. Properties of *Ni-Zn* ferrites can be tailored by substituting them with different metal ions such as Co^{2+}, Mg^{2+}, Mn^{2+}, Cu^{2+} etc. *Ni-Zn* ferrites are one of the most versatile, low cost magnetic materials for general use in both low-and high-frequency devices because of their high resistivity, low dielectric losses, mechanical hardness, high Curie temperature and chemical stability. Typical *Ni-Zn* ferrites are sintered satisfactorily only above 1250° C, where their microstructure and properties being difficult to control because of the volatility of *ZnO* at such high temperatures. High sintering temperature may cause anomalous densification, and high power consumption. Hence from the engineering viewpoint, it would be interesting to prepare *Ni-Zn* ferrites with high-permeability and low magnetic loss at lower sintering temperatures. Additives such as *Cu* or other materials can act as sintering aids having low melting point which can effectively reduce the sintering temperature. Addition of *CuO* with *Ni-Zn* ferrites plays a significant role in increasing the sintering density and lowering the sintering temperature [14]. *Ni-Zn* ferrites doped with *CuO* and sintered at low temperature have found to show high density and high permeability than the undoped one. *Ni-Cu-Zn* ferrites have potential applications in the manufacturing of multilayer chip inductor (MLCI) and in telecommunication devices because of their improved electromagnetic properties at high frequency region. These types of ferrites can

be sintered at relatively lower temperatures with high density and high permeability covering a wide range of compositions. Lowering of sintering temperature is important for co-firing the multilayer chips with silver (*Ag*) as well as from energy saving point of view including the cost effectiveness. Many different additives such as V_2O_5, Bi_2O_3, PbO, MoO_3, WO_3, Eu_2O_3, P_2O_5, Li_2O, Na_2O etc having low melting point facilitated to reduce the sintering temperature of these oxide materials due to liquid phase sintering. *Co*-substituted *Ni-Cu-Zn* ferrites have been discussed in Ref. [15]. Factors influencing the initial permeability of such types of ferrites are noted in their work. In Ref. [16], details of the microstructural study of *Ni-Cu-Zn* ferrites shows a strong correlation between the permeability and the volume fraction of the large ferrite grains. Structural, magnetic and electrical studies of *Ni-Cu-Zn* ferrites with the variation of nickel and zinc content have been reported by Reddi et al. [17]. Along with other properties composition dependent initial permeability at room temperature has been discussed by the authors for their potential uses in multilayer chip inductors (MLCI) [17]. Permeability study of the mixture of nanocrystalline and sub-micron powders of *Ni-Cu-Zn* alloys have been presented in Ref. [18]. Recently, in an article, microwave sintering of iron deficient *Ni-Cu-Zn* ferrites has been performed by Reddy et al. [19]. Initial permeability with temperature and nickel concentration has been investigated in their work. Authors suggested that these types of ferrites are suitable for the application in MLCI due to their low temperature sinterability, good magnetic properties and low loss at high frequency [19].

It is well established that iron deficient Ni-Zn ferrites possess higher density, fine grain size, higher temperature stability, better uniformity in the microstructure and outstanding frequency spectra in comparison with stoichiometric and excess iron samples [20]. Introduction of iron deficiency significantly reduces the Fe^{2+} ions in the sample and thereby inhibiting the electron hopping between Fe^{3+} and Fe^{2+} ions which causes to accelerate the sintering and densification [21]. It is the fact that the decrease iron content from the stoichiometric value effectively lowers the sintering temperature [22]. We also assume that nickel ions are partially replaced by copper ions, based on the concept of reducing the sintering temperature as low as possible and enhancing the permeability as high as possible. We also believe that the Ni^{2+} ions go into octahedral B-sites and replace an equal number of Fe^{3+} ions which move into the tetrahedral A-sites while nonmagnetic Zn^{2+} ions remain in the A-sites. Introduction of little amount of iron deficiency might also produces some vacancies which in turn results in an increase of the mean distance between the magnetic ions. Finally, due to this larger mean distances redistribution of A and B-sites are of obvious. Thus, new types of magnetic interactions are taking place which

eventually causing to increase the magnetic properties of our samples. Even though iron content in ferrites play the crucial role in controlling the electromagnetic and dielectric properties however, until now investigations on iron deficient ferrites are very rare in the literature [23-25]. Thus, there are many scopes to carry out systematic research for more comprehensive understanding various properties of iron deficient ferrites. Keeping these facts in our mind, in the present work, we have discussed the behavior of complex permeability and relevant parameters during the heating and cooling cycles with respect to the variation of temperature and frequency. Furthermore, variation of *Cu*, *Zn* and *Fe* has been maintained in such a way so that high permeability and low magnetic losses along with a low sintering temperature is ascertained. Amount of *Fe*-deficiency was maintained in such way to ensure high permeability as a prime requisite of good inductors.

Experimental Details

Ni-Cu-Zn ferrite powders with composition of $Ni_{0.28}Cu_{0.10}Zn_{0.62}O(Fe_2O_3)_{1-x}$, where x = 0.00, 0.02, 0.04, 0.06 and 0.8 were prepared by ceramic technology using nanoparticles of *NiO*, *CuO*, *ZnO* and Fe_2O_3 with average particle size between 30-50 nm. Many different synthesis techniques are widely used with various dopants around the world to produce ferrites with improved properties suitable for many kinds of technological applications. In this work, conventional ceramic technology has been used for the production of *Ni-Cu-Zn* ferrites for its simplicity and availability. Sample preparation and sintering facility in the laboratory of Materials Science Division (MSD), Atomic Energy Centre Dhaka (AECD) Bangladesh has been used for this purpose. Appropriate proportions of raw materials were weight, mixed, crushed, grinded and milled. Mixing was done by agate motor for about 5 hours and then the materials were crushed. Ball milling was carried out in ethyl alcohol to enhance the degree of mixing. To make mixture homogeneous ball milling was done for 10 hours using steel ball to the powder ratio 1:6 in distilled water. The slurry was dried and the powder was pressed into disc shaped. The disc shape sample was presintered at a constant temperature of 1200^0 C for 5hrs. After that samples were crushed again and subsequently wet ball milled for 6hrs. Presintering was done using a furnace named Gallen Camp. Presintered samples were crushed and the mixtures were milled again using ceramic motor and pestle for 3-4 hours. Using die-punch assembly of hydraulic press under a pressure of 1.70 and 1.15 ton/cm^{-2} different shapes of dies was used to prepare different types of samples. The final products were sintered at constant temperature of 1300^0 C in air for 4 hours and cooled inside the furnace. A constant heating and cooling rate of 5^0

C/min has been maintained throughout the sintering process. The entire ferrite preparation methodology can be described by the following flow chart.

Phase identification and purity level of the samples were confirmed by X-ray diffraction (XRD) studies performed by Philips (PW 3040) X'PERT PRO X-ray diffractometer using Cu-K_α radiation (λ = 1.5418 Å) in the range of 2θ = 20° to 65° in steps of 0.02°. Temperature dependence of initial permeability of the toroidal shaped samples was measured with the Hewlett Packard impedance analyzer (HP 4192A). The frequency dispersion of initial permeability of polycrystalline ferrites is very useful in determining the high frequency characteristics for their potential applications in many devices [26].

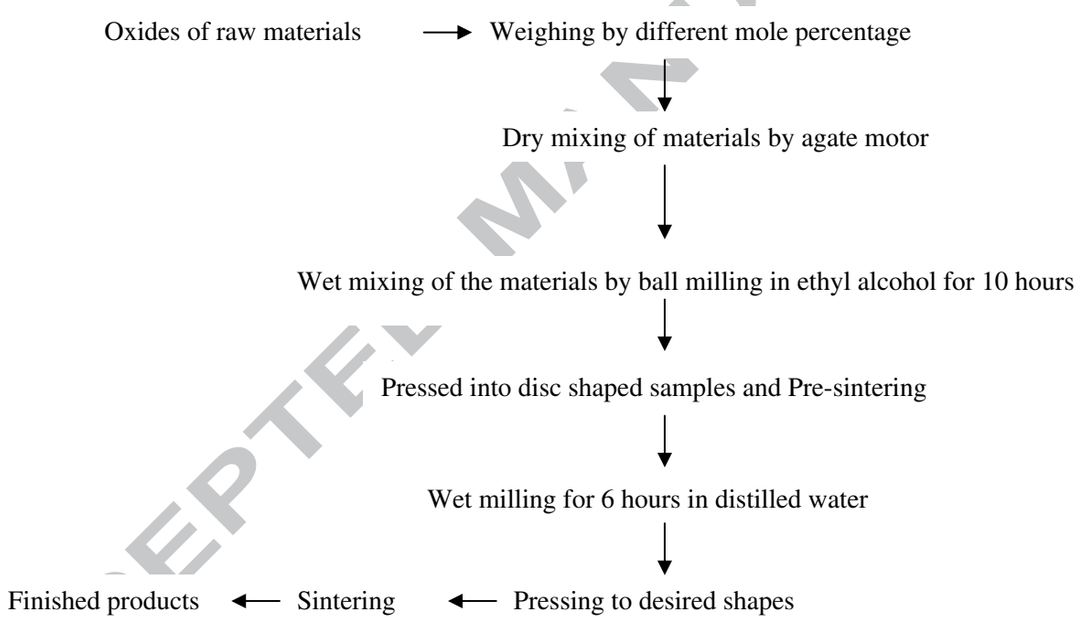

The complex permeability is given by the relation [27]:

$$\mu = \mu' - i\mu'' \qquad (1)$$

where μ' is the real part of the initial permeability that describes the stored energy defining the component of magnetic induction B in phase with the ac applied field H and μ'' represents the imaginary part of the permeability expressing the loss of electric and magnetic energy with the magnetization 90^0 out of phase with the applied magnetic field. The real and imaginary parts of the complex permeability are defined as follows:

$$\mu' = \frac{B_0}{H_0}\cos\delta \qquad (2)$$

$$\mu'' = \frac{B_0}{H_0}\sin\delta \qquad (3)$$

Since the real part μ' of complex permeability represents the component of B which is in phase with H, it corresponds to the normal permeability. In the absence of any losses, $\mu = \mu'$. The presence of imaginary part μ'' requires a supply of energy to maintain the alternating magnetization, regardless of the origin of delay. It is useful to introduce the loss tangent (tanδ). The ratio of μ'' to μ' gives the loss tangent

$$\frac{\mu''}{\mu'} = \frac{\frac{B_0}{H_0}\sin\delta}{\frac{B_0}{H_0}\cos\delta} = \tan\delta \qquad (4)$$

The quality factor (Q-factor) is the reciprocal of the loss tangent defined by the following relation:

$$Q = \frac{1}{\tan\delta} \qquad (5)$$

Results and discussion

Phase analysis of the samples was performed to confirm the formation of single-phase cubic spinel structure using XRD technique which has been displayed in Fig. 1. XRD studies of all the samples of $Ni_{0.28}Cu_{0.10}Zn_{0.62}O\ (Fe_2O_3)_{1-x}$ with (hkl) values corresponding to the diffraction peaks of different planes (111), (220), (311), (222), (400), (422), (511) and (440), which represent either odd or even indicating that the samples are in spinel phase. According to the XRD data, it has been observed that all the samples show good crystallization with well defined diffraction lines without having any other intermediate phases that confirms the formation of single phase spinel structure.

Figs. 2 and 3 show the temperature dependence of the real part of the complex initial permeability of $Ni_{0.28}Cu_{0.10}Zn_{0.62}O\ (Fe_2O_3)_{1-x}$ ferrites at T_s = 1150° C during heating and cooling cycles respectively. Measurements of complex permeability of all the samples in the series has been performed at room temperature using conventional technique based on a circuit loaded with toroidal shaped sample. Observing the variations of permeability with temperature during the heating and cooling processes the Curie temperature, T_c of the samples was calculated. T_c values of all the samples has been presented in Table 1. Figs. 4 and 5 show the temperature dependence of the imaginary part of the complex permeability of the same sample sintered at 1150° C during heating and cooling cycles respectively. At this point, it is very interesting to note that there is

peak value of imaginary part of the complex permeability, μ'' at a particular temperature which has been identified at the peak temperature, T_p. In fact, at this particular temperature μ'' has been found to fall suddenly. Thus, we believe that this peak temperature, T_p corresponds to the Curie temperature, T_c complete spin disorder of the samples take place. Sharp falling of permeability also confirms the purity, homogeneity and single phase of the samples. T_c values of iron deficient *Ni-Cu-Zn* ferrites have been calculated from both the heating and cooling cycles. Figs. 6 and 7 show the variation of T_c of the samples with the increase in iron deficiency during the heating and cooling cycles respectively. From Figs. 6 and 7, it has been observed that T_c increases with the introduction of iron deficiency up to x = 0.06 and then decreases. In both graphs, either in heating or in cooling, T_c has been found to show the highest value at x = 0.06. It is known that at T_c, the thermal energy wining over the exchange energy which results to disorder the system from an ordered one i.e., a ferrimagnetic substance transforms to a paramagnetic one. Curie temperature of ferrites is dependent on the strength of A-B interaction [28]. With the introduction of iron-deficiency, the magnetic moment on A-site might be decreased first which in turn weaken the A-B interaction. Due to this decrease in A-B exchange interaction, the value of T_c is decreased first. Later on, as the iron deficiency is increased on the sample the strength of the interactions between the tetrahedral A-sites and octahedral B-sites might be increased which reveals to enhance the Curie temperature. Our results have been have been found to be consistent with earlier results reported in Ref. [29] for Cd-Cr-Cu ferrites. According to the T_c data, it reveals that T_c data during heating and cooling are very close to each other in both cases. Small differences in the T_c measurements in heating and cooling processes may occur due to the reduced thermal disturbance taking place during the cooling cycle.

The real part of the initial permeability is directly proportional to the square of the magnetization and inversely proportional to the anisotropy constant of the samples (see Eq. (7)). Since the anisotropy decreases faster than the magnetization during the heating cycle, the permeability is decreased with the rise in temperature tends to infinity just below the Curie temperature and then falls sharply to low value and the sample becomes a paramagnetic one. In our investigation, all the samples exhibited thermal hysteresis with Hopkinson's peaks following the relation $\mu'_{cooling}$, $\mu''_{cooling} > \mu'_{heating}$, $\mu''_{heating}$ (see Figs. 2, 3, 4 and 5) where $\mu'_{cooling}$ and $\mu''_{cooling}$ are the real and imaginary part of the initial permeability near the Hopkinson's peak during the cooling cycle while $\mu'_{heating}$ and $\mu''_{heating}$ is the real and imaginary part of the initial permeability near the Hopkinson's peak during the heating process respectively. Similar types of results for the

thermal hysteresis have been reported in Cu-Mg-Zn ferrites [30-31] and Ni-Zn ferrites [32]. A slight deviations in the magnitudes of the real part of the initial permeability of *Ni-Cu-Zn* ferrites recorded during the heating and cooling processes occur might be due to the decrease in thermal disturbance on cooling. This might be also related to the resultant magnetization on effective ordering of the domains present in the grains.

Initial permeability has been found to be related with magnetization and ionic structure, thereby the thermal spectra of permeability can be also considered as a test of the formation and homogeneity of the ionic structure of the samples. The temperature dependence of the permeability can be explained in terms of the Hopkinson's effect [33-34]. According to the Eq. (7), it is clearly observed that the permeability is directly proportional to the square of M_s and inversely proportional to the anisotropy constant, K of the materials. As the temperature is increased both K and M_s are decreased. However, the rate of decrease of anisotropy constant is faster than that of the saturation magnetization. For this reason, permeability enhances very fast around T_c (the ferro/paramagnetic transition temperature of the sample) [33-34]. The initial permeability of ferrites depends on many factors such as reversible domain wall displacement, domain wall bulging as well as microstructural features viz., intragranular porosity, chemical composition, average grain size and the presence of second phase etc [35]. At high sintering temperature and frequency, the initial permeability decreases due to the decrease in average grain size of the samples. As a result, removal of the domain wall pinning sites at the grain boundary is also increased. Presence of Cu-content rich precipitation and porosity could also come into play to pin the domain wall and causing to reduce the initial permeability at higher sintering temperature and frequency.

In earlier investigations it has been reported that for soft ferrites the permeability and grain size are directly proportional to each other i.e., $\mu' \propto D$ [10, 36-38]. Eq. (6) also shows that permeability due to the motion of the domain wall is remarkably influenced by the grain size. Since the initial permeability is measured as a result of the easy reversal of domain wall displacement in the direction of the applied field and bigger grains accommodate more domains, the larger the number of domain walls the higher the permeability is. It is the fact that the average grain size of the sample increases with the rise in sintering temperature. Thus, for a large grain permeability will increase as it changes proportionally with the diameter of the grain. That means higher initial permeability is expected at high T_s. However, in our study, it has been

noticed that for the samples real part of the initial permeability found to be highest at an optimum sintering temperature (see Figs. 9). If the sample be sintered higher than the optimum T_s, the real part of the initial permeability is decreased (see Fig. 10). This could be explained based on the fact that samples sintered at ≥ optimum T_s may increase the number of pores in the grains which in turn causes to decrease of μ′. Our investigations have been found to be consistent with earlier reports on Mn-Zn ferrites [39]. A linear relationship between the grain size and permeability is valid until the grain growth is normal, i.e., if all the grains grow pretty much at the same time and same rate. However, the pores generated at the grain boundaries are less damaging to the permeability because it causes less hindrance to domain wall motion than that within the grains. Permeability of soft ferrites is related to the spin rotation and domain wall motion [40-41]. Spin rotation and domain wall motion are related as $\mu = 1+ \chi_w + \chi_{spin}$, where χ_w is the domain wall susceptibility, χ_{spin} is the intrinsic rotational susceptibility. The domain wall susceptibility and the intrinsic rotational susceptibility are given by the following Eqs.

$$\chi_w = \frac{3\pi M_s^2 D}{4\gamma} \quad (6)$$

$$\chi_{spin} = \frac{2\pi M_s^2}{K} \quad (7)$$

where M_s, K, D and γ are the saturation magnetization, total anisotropy, average grain diameter, and domain wall energy respectively. Properties of soft ferrites are dependent on their compositions, additives and microstructures. It is well known that the magnetic properties are greatly influenced by the microstructures; the larger the grain sizes, the higher the saturation magnetization and larger initial permeability. Ferrites with lower initial permeability and saturation magnetization are suitable for microwave applications.

Figs. 8, 9 and 11 shows the variation of the real part of the complex initial permeability of iron deficient *Ni-Cu-Zn* ferrites with frequency sintered at 1100° C, 1150° C and 1200° C respectively while the imaginary part of the complex permeability of the same samples have been shown in Figs. 12, 13 and 14. All the measurements have been done using Hewlett Packard Impedance Analyzer (Model No. HP 4192A) in the frequency range of 1 kHz to 13 MHz at room temperature. The permeability values of the *Ni-Cu-Zn* ferrites sintered at 1100° C, 1150° C and 1200° C with introduction of iron deficiency have been presented in Table 1 along with the resonance frequency. From Figs. 8-14, it is clearly evident that the permeability increases significantly with the increase in iron-deficiency to the pure sample. This is attributed to the fact that the density of the samples is increased which leads to an increase the permeability. It is

earlier mentioned that ferrites with higher density and larger average grain size have a higher initial permeability [42]. A comparative study of the permeability spectra of iron deficient *Ni-Cu-Zn* ferrites at a constant frequency (f = 100 kHz) sintered at 1100° C, 1150° C and 1200° C has been presented in Fig. 11. Fig. 11 shows that samples sintered at 1200° C have lower permeability than that sintered at 1150° C. According to our study, it has been also observed that the permeability of the sample sintered at 1150° C showing the highest magnitude. This reveals that the sample sintered at this temperature shows better magnetic properties comparing to the others. Since, the intension of adding *Cu* with the samples is work as a sintering aid; this has been confirmed by showing highest permeability at lower sintering temperature while the permeability has been found to be decreased for the samples sintered at 1200° C. A comparative study of the permeability spectra of iron deficient Ni-Cu-Zn ferrites with frequency sintered at 1100° C, 1150° C and 1200° C has been presented in Fig. 11. Fig. 11 shows that samples sintered at 1200° C have lower permeability than that sintered at 1150° C. From Fig. 11, it could be also mentioned that the permeability of the sample with $x = 0.08$ is decreased. This reveals the formation of significant amount of non-magnetic phases which in turn causes to decrease in permeability of the iron deficient sample [18].

Throughout the study, it was recorded that the real part of the initial complex permeability remains fairly unchanged over a large range of frequency and then decreases sharply at very high frequency. However, the imaginary part of the permeability gradually increases with the increase in frequency, took a broad maximum at a certain frequency (see Figs. 12-14) while the real part has been observed to be decreased. This type of feature is known as the ferrimagnetic resonance [43-44]. The permeability increases with a decrease in K, according to the relation $\mu \approx \frac{M_s}{\sqrt{K}}$ [45]. High permeability in the low frequency side remarkably show the dominant role played by the motion of the domain wall. In addition, in the low frequency region, ferrites work as a low loss constant self-inductor where the core is mostly inductive and thereby rejects electromagnetic interference signal to the source. On the other hand, in the high frequency side, inductive core show high impedance and becomes more resistive and dissipates the interfering signals rather than reflecting these to the source [46]. Resonance peaks are the results of the absorption of energy due to the coincidence of the frequency of the magnetic dipoles and applied field. At resonance, highest amount of energy is transmitted from the applied ac magnetic field to the lattice. It might also be explained using the fact that at high frequency side, magnetization of the sample cannot follow the frequency of the applied ac field. Moreover, in the high frequency

region, permeability has been found to be governed by the spin rotation due to the damping of the domain walls. Spins are relaxed at higher frequencies which in turn cause to reduce the permeability to a lower value. Considering this facts a perfect frequency band can be successfully identified at which the sample can be used. From permeability of shown in Figs. 8, 9, 10 and 12 it is also observed that the higher the permeability the lower the resonance frequency. This behavior of our sample proofs the validity of the Snoek's model [47] that defines the relationship between resonance frequency and initial permeability as $f_r \mu' = \text{constant}$, where f_r is the resonance frequency for the domain wall motion above which initial permeability, μ' gets decreased. That is the product of initial permeability and resonance frequency always remains constant. The lower the permeability values, the higher the frequencies at which resonance will take place. This way, an effective limit of the product of these two parameters (high f_r and high μ') could be identified so that the pair is mutually incompatible.

Frequency characteristics of the relative quality factor (Q-factor) of iron deficient Ni-Cu-Zn ferrites sintered at 1150° C has been displayed in Fig. 15. Relative Q-factor calculated from the loss tangent measured on the coil wound toroidal shaped samples. All the samples have been found to show similar trend with the frequency. The Q-factor increases with the rise in frequency showing a sharp maximum and then starts decreasing with the further increase in frequency. From the relative Q-factor data, it is also noticed that the relative Q-factor of the samples decreases with the increase in iron deficiency. Highest value of the relative Q-factor of iron deficient Ni-Cu-Zn ferrites was recorded at $x = 0.00$. Peaks corresponding to the maxima in Q-factor were shifted towards the higher frequency side with the increase in iron deficiency to the samples. Generally, the loss of energy is related to various domain defects such as non-uniform and non-repetitive domain wall motion, domain wall bowing, localized variation of the flux density and nucleation and annihilation of domain walls [48]. Moreover, in ferrites losses might also arise due to other factors: eddy current loss, hysteresis loss, and residual loss [40]. Eddy current losses can be minimized by increasing the resistivity of ferrites. Since the resistivity of ferrites depends on the composition, sintering environment, and cooling rate [40]. Thus, a slow cooling rate is essential to reduce the trapping of pores within grains which in turn reduces the eddy current losses. Hysteresis loss mainly contributes by the irreversible wall displacements found to be increased by the increase of grain size and the impurity in the raw materials [49]. Residual losses have been found to arise due to the relaxation of domain walls [49]. All the phenomena of losses come into play when the permeability begins to drop which is well known

as the ferrimagnetic resonance [50]. At resonance, maximum amount of energy is transformed from the applied ac magnetic field to the lattice and thus resulting in a quick decrease in relative Q-factor.

Conclusions

The influence of Fe deficiency on the temperature and frequency dependent complex permeability and relevant parameters of $Ni_{0.28}Cu_{0.10}Zn_{0.62}O(Fe_2O_3)_{1-x}$ ferrites, where x = 0.00, 0.02, 0.04, 0.06 and 0.08 prepared by the conventional ceramic technique have been investigated. Effect of sintering temperatures on the complex permeability and other relevant properties have been also discussed in this work. The temperature dependence of the initial complex permeability measurements have been found to execute the good peaking behavior at the transitions temperatures (T_c). In our study, Curie temperature increases with increase of Fe-deficiency to the pure *Ni-Cu-Zn* ferrites. The permeability of the samples was found to be increased significantly with the introduction of iron deficiency. The flat trend of the permeability spectra of our samples up to a large frequency range indicate the potential device applications of these materials. Since the permeability spectra of soft magnetic materials are strongly dependent on the preparation conditions and sintering environment, it was observed that samples sintered at higher temperatures show ascending tendency of the initial permeability. However, above an optimum temperature the permeability recorded to be decreased again. For a good magnetic material, primary requirement is the highest possible permeability together with low losses in the frequency range of interest. The increase in the complex initial permeability, increase in Curie temperature and resonant frequency with the increase in Fe deficiency are related to the increase in Ni/Zn ratio derived from the separation of zinc from spinel sample. Therefore, low temperature sintering of Ni-Cu-Zn ferrites can be successfully attained by lowering iron content from the spinel lattice, partially substituting nickel ions by copper ions and thereby reducing the Fe^{2+} in the ferrites.

Acknowledgements

One of the authors (Z.H.K) gratefully acknowledges the financial support of Khulna University of Engineering & Technology, Bangladesh to carry out this work successfully.

References

[1] J. Kulikowski, J. Magn. Magn. Mat., **41**, 56 (1984).

[2] A. Verma, T.C. Goel, R.G. Mendiratta, R.G. Gupta. J. Magn. Magn. Mat., **192**, 271 (1999).
[3] T. Nakamura, T. Miyamoto, Y. Yamada, J. Magn. Magn. Mat., **256**, 340 (2003).
[4] A. Lakshman, K.H. Rao, R.G. Mendiratta., J. Magn. Magn. Mat., **250**, 92 (2002).
[5] N. Rezlescu, L. Rezlescu, P.D. Popa, E. Rezlescu., J. Magn. Magn. Mat., **215-216**, 194 (2000).
[6] H.M. Zaki, S.F. Mansour, Mat. Chem. Phy., **88**, 326 (2004).
[7] E. Rezlescu, L. Sachelarie, P.D. Popa, and N. Rezlescu., IEEE Transactions on Magnetics, **36**, 6 (2000).
[8] M.M. Haque, M Huq and M A Hakim, J. Phy. D: App. Phy., **41**, 055007, 10 (2008).
[9] S.H. Seo and J. H. Oh., IEEE Transactions on Magnetics, **35** (5), (1999).
[10] M.M. Haque, M. Huq, M.A Hakim., J. Magn. Magn. Mat., **320**, 2792 (2008).
[11] J. Bera, P.K., Physica B, **363**, 128 (2005).
[12] K.S. Amarendra, T.C. Goel and R.G. Mendiratta., J. Appl. Phys., **92**, 3872 (2002).
[13] A.A. Sattar, H .M. El-sayed, K.M.EL-Shokrofy and M.M. El-Tabey., J. Appl. Sci., **5** (1): 162 (2005).
[14] T.T. Ahmed, I.Z. Rahman and S.A.M. Tofail., J. Magn. Magn. Mat., **272-276** (3), 2250 (2004).
[15] T.Y. Byun, S.C. Bycon**,** K.S. Hong, C.K. Kim, IEEE Trans. Magn., **35**(5), 3445 (1999).
[16] T. Rabe, H. Naghib-zadeh, C. Glitzky and J. Töpfer, Int. J. Appl. Ceram. Technol., **9** (1), 18 (2012).
[17] M.P. Reddy, G. Balakrishnaiah, W. Madhuri, M.V. Ramana, N.R. Reddy, K.V.S. Kumar, V.R.K. Murthy, R.R. Reddy, J. Phys. Chem. Sol., **71**(9), 1373 (2010).
[18] J. Mürbe, J. Töpfer, J. Euro. Ceram. Soc., **32**(5), 1091 (2012).
[19] M.P. Reddy, W. Madhuri, G. Balakrishnaiah, N.R. Reddy, K.V.S. Kumar, V.R.K. Murthy, R.R. Reddy, Curr. Appl. Phys., **11**(2), 191 (2011).
[20] Z. Ling, M. Xiong, Q. Zhang, J. Magn. Magn. Mater., **219**, 9 (2000).
[21] A. Glubus, R.V. Monjaras, IEEE Trans. Magn., **11**, 1300 (1975).
[22] Kimura, O., Matsumoto, M. and Sakakura, M., *J. Am. Ceram. Soc.*, **78**, 2857 (1995).
[23] Xinhua He, Zhide Zhang, Zhiyuan Ling, Ceram. Intl., **34**, 1409 (2008).
[24] X. He, G. Song, J. Zhu, Mater. Lett., **59**, 1941 (2005).
[25] R.V. Mangalaraja, P. Manohar, F.D. Gnanam, J. Mater. Sci., **39**, 2037 (2004).
[26] T. Tustaoka, T. Nakamura and K. Hatakeyama, J. Appl. Phys., **78** (6), 3983 (1995).
[27] S.M. Hoque, M.S. Ullah, F.A. Khan, M.A. Hakim and D.K. Saha, Physica B., **406**, 1799 (2011).
[28] A.M. Shaikh S.C. Watawe, S.A. Jadhav, B.K. Chougule, Mater. Research Bull., **37**, 2547 (2002).
[29] C. Greskovich, K.W. Lay, J. Am. Ceram. Soc., **55**, 142 (1972).
[30] D.N. Bhosale, S.R. Sawant, S.A. Gangal, R.R. Mahajan, P.P. Bakare, Mater. Sci. Engg. B., **65**, 79 (1999).
[31] D.N. Bhosale, N.D. Chaudhari, S.R. Sawant, P.P. Bakare, J. Magn. Magn. Mater., 173, 51 (1997).
[32] J.D. Loaec, J. Phys. D: Appl. Phys., **26**, 963 (1993).
[33] S.M. Hoque, A.K.M. Rezaul Haque, M.O. Rahman, N.H. Nghi, J. Noncrys. Sol., **357,** 2109 (2011).
[34] S.K. Nath, K.H. Maria, S. Noor, S.S. Sikder, S.M. Hoque and M.A. Hakim, J. Magn. Magn. Mater., **324**, 2116 (2012).
[35] J. Smit, H.P.J. Wijin, Ferrites, Philips Tech. Library, Netherlands, (1959).

[36] S.V. Kakatkar, S.S. Kakatkar, R.S. PAtil, A.M. Sankpal, N.D. Chaudhari, P.K. Maskar, S.S. Suryawanshi, S.R. Sawant, Mater. Chem. Phys., **46**, 96 (1996).
[37] D.J. Perduijin, H.P. Peloschek, Proc. Brit. Ceram. Soc., **10**, 263 (1968).
[38] E. Roess, I. Hanke and E. Moser, Z. Angew. Phys., **17**, 504 (1964).
[39] C. Guillaud,Proc. IEEE, **104** B, 165 (1957).
[40] J. Smit and Wijin H. P. J. Ferrites (1959).
[41] H. Jun, Y. Mi, J. Zhejiang, Univ. Sc. **6**B (6), 580 (2005), 580.
[42] E.C. Snelling, Proceedings, ICF-5, India 579, (1989).
[43] T. Nakamura, J. Appl. Phys., **88**, 348 (2000).
[44] K.O. Low and F.R. Sale, J. Magn. Magn. Mater., **246**, 30 (2002).
[45] R. Valenzuela, Magnetic Ceramic, Cambridge University Press, Cambridge, (1994).
[46] E.C. Snelling, Soft Ferrites: Properties and Applications (2nd Edition), Butterworth, London (1988).
[47] J.L. Snoek, Physica **14** (4), 207 (1948).
[48] K.J. Overshott, IEEE Trans. Magn., **17**, 2698 (1981).
[49] S.S. Bellad, B.K. Chougule, Mater. Chem. Phys., **66**, 58 (2000).
[50] F.G. Brockman, P.H. Dowling and W.G. Steneck, Phys. Rev., **77**, 85 (1950).

FIGURE Captions

Figure 1: XRD pattern of $Ni_{0.28}Cu_{0.10}Zn_{0.62}O$ $(Fe_2O_3)_{1-x}$ ferrites sintered at 1150° C in air for 3 hours.

Figure 2: Temperature dependence (Heating) of the real part of the initial permeability, μ′ of $Ni_{0.28}Cu_{0.10}Zn_{0.62}O$ $(Fe_2O_3)_{1-x}$ ferrites at T_s = 1150° C.

Figure 3: Temperature dependence (Cooling) of the real part of the initial permeability, μ′ of $Ni_{0.28}Cu_{0.10}Zn_{0.62}O$ $(Fe_2O_3)_{1-x}$ ferrites at T_s = 1150° C.

Figure 4: Temperature dependence (Heating) of the imaginary part of the initial permeability, μ′ of $Ni_{0.28}Cu_{0.10}Zn_{0.62}O(Fe_2O_3)_{1-x}$ ferrites at T_s = 1150° C.

Figure 5: Temperature dependence (Cooling) of the imaginary part of the initial permeability, μ′ of $Ni_{0.28}Cu_{0.10}Zn_{0.62}O(Fe_2O_3)_{1-x}$ ferrites at T_s = 1150° C

Figure 6: Variation of Curie temperature (Heating & Cooling) as a function of x for $Ni_{0.28}Cu_{0.10}Zn_{0.62}O$ $(Fe_2O_3)_{1-x}$ ferrites at T_s = 1150° C.

Figure 7: Variation of the peak temperature T_p (Heating & Cooling) as a function of x for $Ni_{0.28}Cu_{0.10}Zn_{0.62}O(Fe_2O_3)_{1-x}$ ferrites at T_s = 1150° C.

Figure 8: Frequency dependence of the real part of the permeability, μ′ as a function of frequency of $Ni_{0.28}Cu_{0.10}Zn_{0.62}O$ $(Fe_2O_3)_{1-x}$ ferrites sintered at 1100° C.

Figure 9: Frequency dependence of the real part of the permeability, μ′ as a function of frequency of $Ni_{0.28}Cu_{0.10}Zn_{0.62}O$ $(Fe_2O_3)_{1-x}$ ferrites sintered at 1150° C.

Figure 10: Frequency dependence of the real part of the permeability, μ′ as a function of frequency of $Ni_{0.28}Cu_{0.10}Zn_{0.62}O$ $(Fe_2O_3)_{1-x}$ ferrites sintered at 1200° C.

Figure 11: Variation of the real part of the permeability, μ′ of $Ni_{0.28}Cu_{0.10}Zn_{0.62}O$ $(Fe_2O_3)_{1-x}$ ferrites with Fe-deficient at different sintering temperatures.

Figure 12: Imaginary part of complex initial permeability, μ″ as a function of frequency of $Ni_{0.28}Cu_{0.10}Zn_{0.62}O(Fe_2O_3)_{1-x}$ ferrites sintered at 1100° C.

Figure 13: Imaginary part of complex initial permeability, μ″ as a function of frequency of $Ni_{0.28}Cu_{0.10}Zn_{0.62}O(Fe_2O_3)_{1-x}$ ferrites sintered at 1150° C.

Figure 14: Imaginary part of complex initial permeability, μ″ as a function of frequency of $Ni_{0.28}Cu_{0.10}Zn_{0.62}O(Fe_2O_3)_{1-x}$ ferrites sintered at 1200° C.

Figure 15: Frequency dependence of relative Q-factor of $Ni_{0.28}Cu_{0.10}Zn_{0.62}O(Fe_2O_3)_{1-x}$ ferrites sintered at 1100° C.

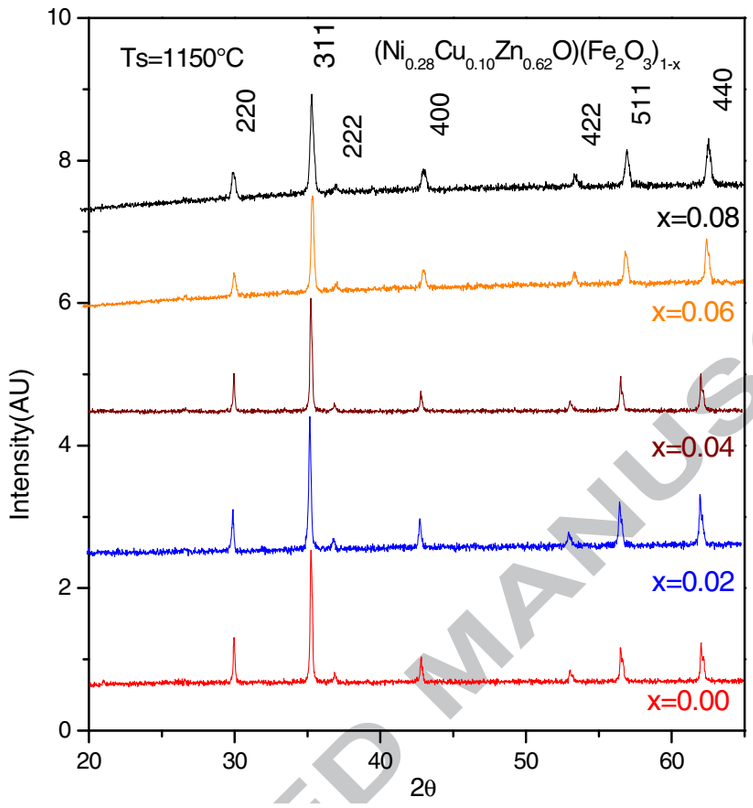

Figure 1: XRD pattern of $Ni_{0.28}Cu_{0.10}Zn_{0.62}O$ $(Fe_2O_3)_{1-x}$ ferrites sintered at 1150° C in air for 3 hours.

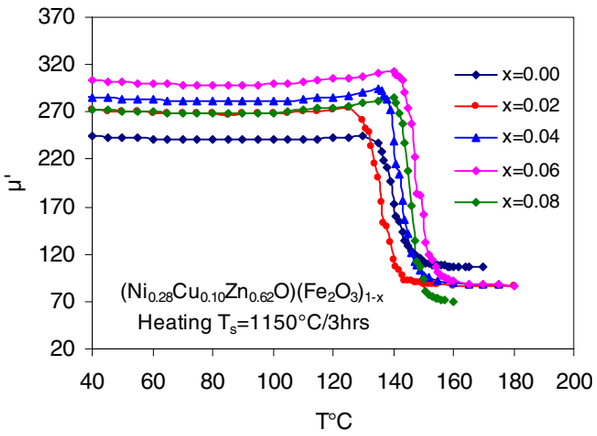

Figure 2: Temperature dependence (Heating) of the real part of the initial permeability, μ′ of $Ni_{0.28}Cu_{0.10}Zn_{0.62}O$ $(Fe_2O_3)_{1-x}$ ferrites at T_s = 1150° C.

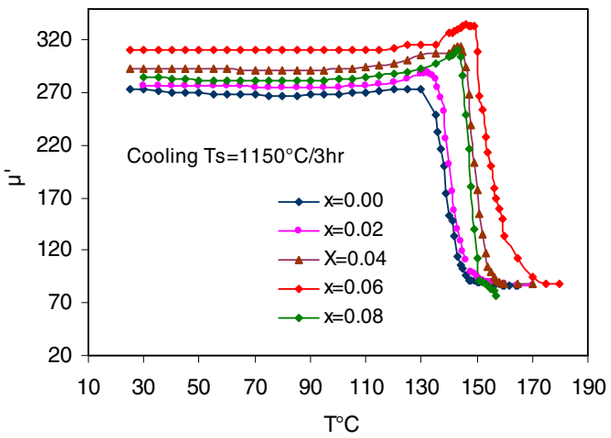

Figure 3: Temperature dependence (Cooling) of the real part of the initial permeability, μ′ of $Ni_{0.28}Cu_{0.10}Zn_{0.62}O$ $(Fe_2O_3)_{1-x}$ ferrites at T_s = 1150° C.

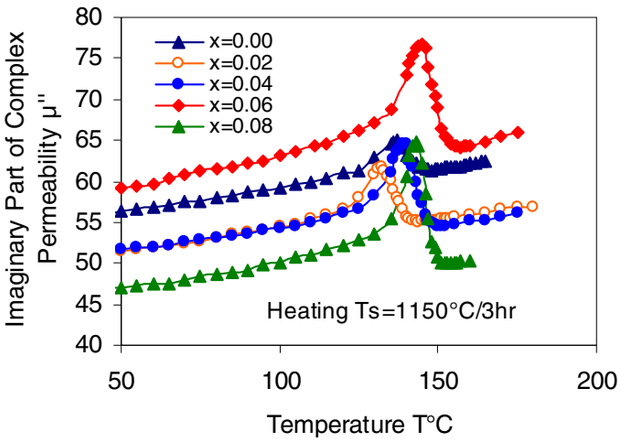

Figure 4: Temperature dependence (Heating) of the imaginary part of the initial permeability, μ′ of $Ni_{0.28}Cu_{0.10}Zn_{0.62}O(Fe_2O_3)_{1-x}$ ferrites at T_s = 1150° C.

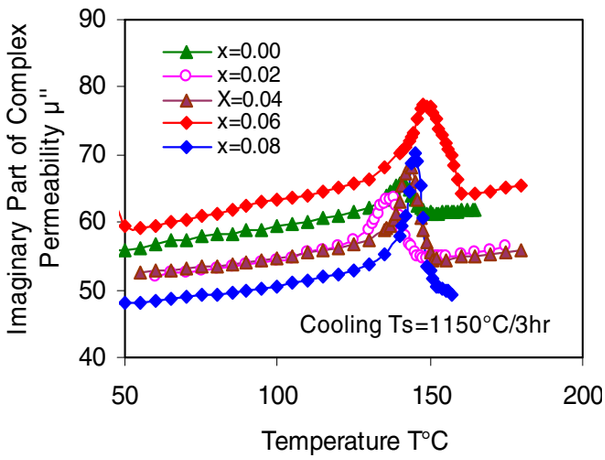

Figure 5: Temperature dependence (Cooling) of the imaginary part of the initial permeability, μ′ of $Ni_{0.28}Cu_{0.10}Zn_{0.62}O(Fe_2O_3)_{1-x}$ ferrites at T_s = 1150° C

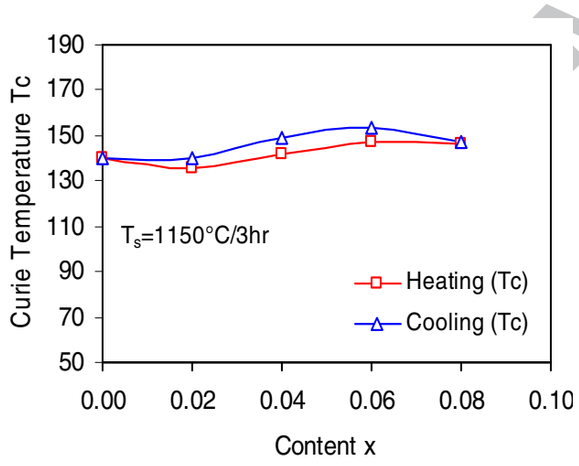

Figure 6: Variation of Curie temperature (Heating & Cooling) as a function of x for $Ni_{0.28}Cu_{0.10}Zn_{0.62}O(Fe_2O_3)_{1-x}$ ferrites at T_s = 1150° C.

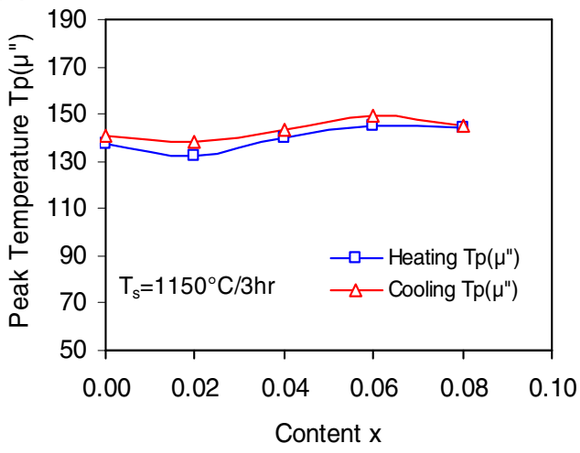

Figure 7: Variation of the peak temperature T_p (Heating & Cooling) as a function of x for $Ni_{0.28}Cu_{0.10}Zn_{0.62}O(Fe_2O_3)_{1-x}$ ferrites at T_s = 1150° C.

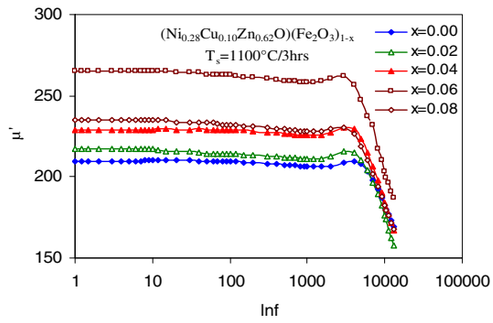

Figure 8: Frequency dependence of the real part of the permeability, μ′ as a function of frequency of $Ni_{0.28}Cu_{0.10}Zn_{0.62}O$ $(Fe_2O_3)_{1-x}$ ferrites sintered at 1100° C.

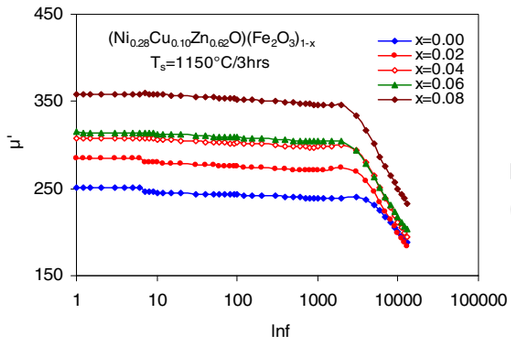

Figure 9: Frequency dependence of the real part of the permeability, μ′ as a function of frequency of $Ni_{0.28}Cu_{0.10}Zn_{0.62}O$ $(Fe_2O_3)_{1-x}$ ferrites sintered at 1150° C.

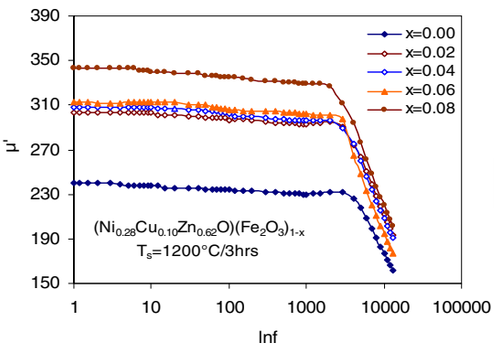

Figure 10: Frequency dependence of the real part of the permeability, μ′ as a function of frequency of $Ni_{0.28}Cu_{0.10}Zn_{0.62}O$ $(Fe_2O_3)_{1-x}$ ferrites sintered at 1200° C.

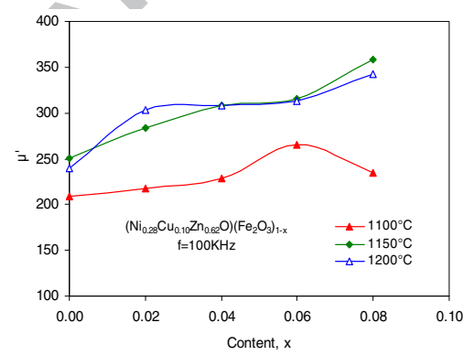

Figure 11: Variation of the real part of the permeability, μ′ of $Ni_{0.28}Cu_{0.10}Zn_{0.62}O$ $(Fe_2O_3)_{1-x}$ ferrites with Fe-deficient at different sintering temperatures.

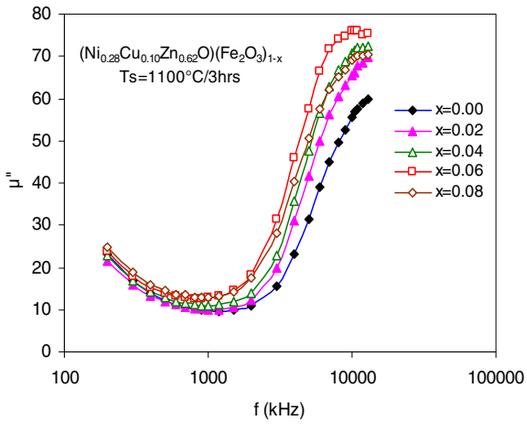

Figure 12: Imaginary part of complex initial permeability, μ″ as a function of frequency of $Ni_{0.28}Cu_{0.10}Zn_{0.62}O(Fe_2O_3)_{1-x}$ ferrites sintered at 1100° C.

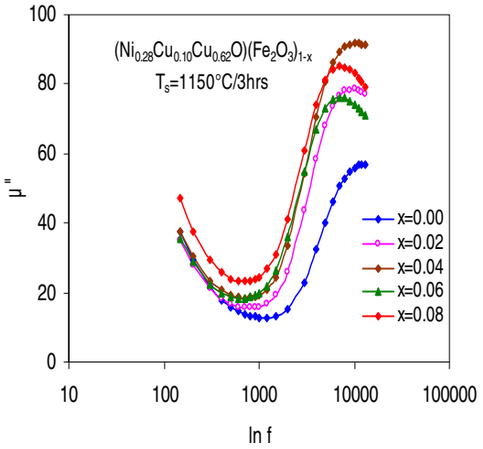

Figure 13: Imaginary part of complex initial permeability, μ″ as a function of frequency of $Ni_{0.28}Cu_{0.10}Zn_{0.62}O(Fe_2O_3)_{1-x}$ ferrites sintered at 1150° C.

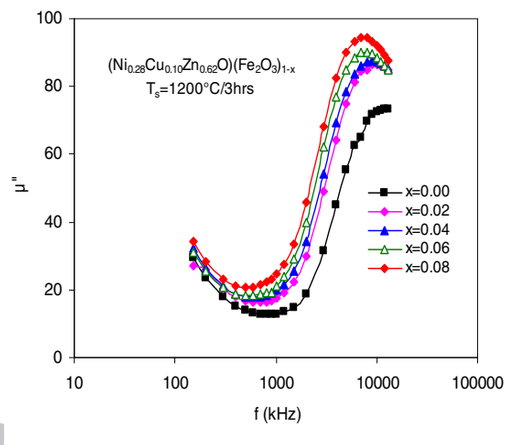

Figure 14: Imaginary part of complex initial permeability, μ″ as a function of frequency of $Ni_{0.28}Cu_{0.10}Zn_{0.62}O(Fe_2O_3)_{1-x}$ ferrites sintered at 1200° C.

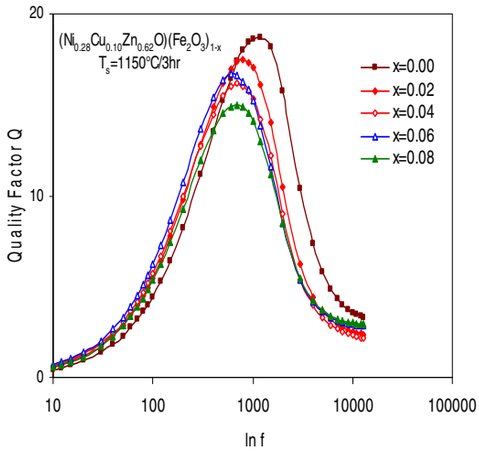

Figure 15: Frequency dependence of relative Q-factor of $Ni_{0.28}Cu_{0.10}Zn_{0.62}O(Fe_2O_3)_{1-x}$ ferrites sintered at 1100° C.

Table Caption

Table 1: Curie temperature, initial permeability and resonance frequency of $Ni_{0.28}Cu_{0.10}Zn_{0.62}O(Fe_2O_3)_{1-x}$ ferrites, where x = 0.00, 0.02, 0.04, 0.06 and 0.08.

Table 1: Curie temperature, initial permeability and resonance frequency of $Ni_{0.28}Cu_{0.10}Zn_{0.62}O(Fe_2O_3)_{1-x}$ ferrites, where x = 0.00, 0.02, 0.04, 0.06 and 0.08.

Amount of iron deficiency, x	Curie Temperature, T_c (^{0}C)	Sintering Temperature, Ts = 1100° C		Sintering Temperature, Ts = 1150° C		Sintering Temperature, Ts = 1200° C	
		Real part of the initial permeability, μ′(at 100kHz)	Resonant frequency, f_r(MHz)	Real part of the initial permeability, μ′(at 100kHz)	Resonant frequency, f_r(MHz)	Real part of the initial permeability, μ′(at 100kHz)	Resonant frequency, f_r(MHz)
0.00	146	209	13	251	12	240	12
0.02	137	217	12	284	10	303	9
0.04	151	229	12	308	10	311	9
0.06	150	265	10.5	316	7	313	8
0.08	151	235	12	358	7	343	7

Highlights of the Present Study

- *Ni-Cu-Zn* ferrites were studied with increase of *Fe*-deficiency.
- Permeability spectra of *Fe*-deficient *Ni-Cu-Zn* ferrites are discussed.
- Heating and cooling cycles are used for the various studies of *Ni-Cu-Zn* ferrites.
- *Fe*-deficiency in *Ni-Cu-Zn* ferrites ensures high permeability.
- Cu works as a sintering aid to the *Fe*-deficient *Ni-Cu-Zn* ferrites.